Supporting Information Appendix for Moiré-less Correlations in ABCA Graphene

Alexander Kerelsky,[1,*] Carmen Rubio-Verdú,[1,*] Lede Xian,[2,3] Dante M. Kennes,[2,4] Dorri Halbertal,[1] Nathan Finney,[5] Larry Song,[1] Simon Turkel,[1] Lei Wang,[1] K. Watanabe,[6] T. Taniguchi,[6] James Hone,[5] Cory Dean,[1] Dmitri Basov,[1] Angel Rubio,[2,7,8,†] and Abhay N. Pasupathy[1,†]

[1] *Department of Physics, Columbia University, New York, New York 10027, United States*
[2] *Max Planck Institute for the Structure and Dynamics of Matter, Luruper Chaussee 149, 22761 Hamburg, Germany*
[3] *Songshan Lake Materials Laboratory, Dongguan, Guangdong 523808, China*
[4] *Institut fur Theorie der Statistischen Physik, RWTH Aachen University, 52056 Aachen, Germany and JARA-Fundamentals of Future Information Technology, 52056 Aachen, Germany*
[5] *Department of Mechanical Engineering, Columbia University, New York, NY, USA*
[6] *National Institute for Materials Science, 1-1 Namiki, Tsukuba 305-0044, Japan*
[7] *Center for Computational Quantum Physics (CCQ), The Flatiron Institute, 162 Fifth Avenue, New York, NY 10010, USA*
[8] *Nano-Bio Spectroscopy Group, Departamento de Fisica de Materiales, Universidad del País Vasco, 20018 San Sebastian, Spain*

(Dated: December 16, 2020)

This PDF file includes:

TINY ANGLE TWISTED BILAYER GRAPHENE

For comparison to small angle twisted double bilayer graphene (tDBG), in Figure S1 we show a small angle twisted bilayer graphene (tBG) STM topography. It is clear from the topography and main text Figure 1D that the contrast is fundamentally different in small angle tDBG as opposed to tBG. The main contrast in tBG emerges from the AA sites and the SP domain walls. In between, there are maximized (in space) commensurate Bernal stacked AB and BA regions which show the same contrast. On the other hand in tDBG the dominant contrast comes from two sets of different commensurate stacking domains – ABAB (Bernal) and ABCA (rhombohedral) graphene as described in the text.

BERRY CURVATURE IN ABCA AND ABAB GRAPHENE

In order to investigate the topological properties of ABCA and ABAB graphene, we calculate the berry curvatures for the low energy bands for the two systems under applied displacement field. We use the tight-binding model calculations with hopping between lattice sites as given in the methods section. To simulate the applied displacement field, the onsite potential difference between adjacent layers is set to be 0.08 eV. Figure S2A shows the Berry curvature calculated for the bottom of the conduction band of ABCA graphene for half of the Brillouin zone centered around the K point. It can be seen that there is a large peak around the K point. If we integrate the Berry curvature around the region close to this K valley, we can obtain a valley Chern number of +2 for the bottom of the conduction band of ABCA graphene.

There is no overall band gap for ABAB graphene even under applied displacement field. However, if we just consider the states at the surface layer (the top or the bottom), there is indeed a band gap between surface bands 1 and 3 (see main text Figure 4C). The Berry curvature calculated for the bottom of conduction band 1 is shown in

* These authors contributed equally to this work.

† Correspondence to: apn2108@columbia.edu (A.N.P); angel.rubio@mpsd.mpg.de (A.R.)

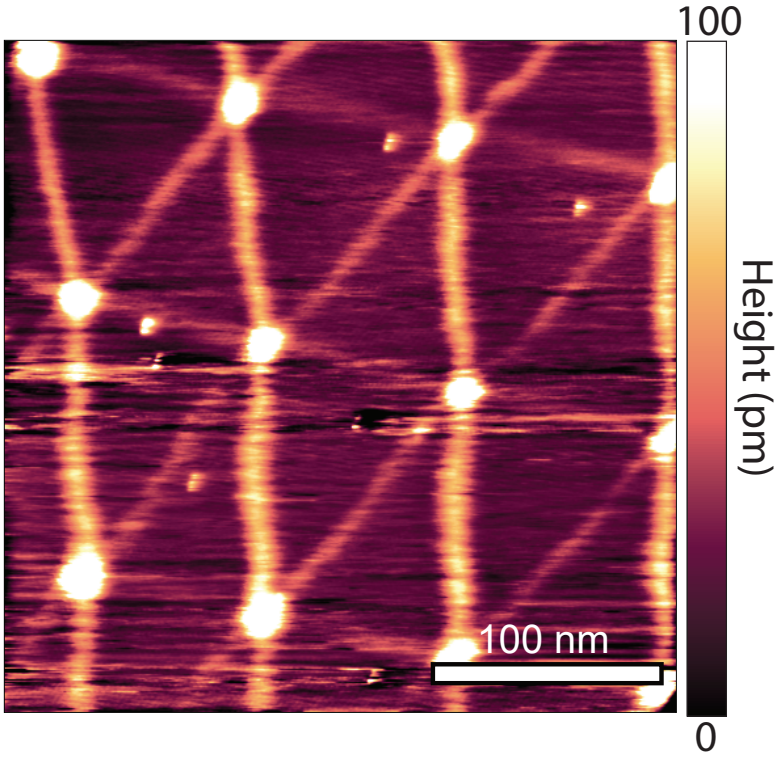

FIG. S1. A small angle twisted bilayer graphene (tBG) moiré. The dominant contrast for small angle tBG comes from the AA sites and the SP domain walls. The AB versus BA commensurate stacking domains show the same contrast unlike the ABAB versus ABCA commensurate stacking domains in small angle tDBG.

Figure S2B. If we integrate the Berry curvature around the region close to the K valley, we obtain a valley Chern number of +1, which is different from the case of ABCA graphene. The difference of the valley Chern number between the surface bands of ABCA and ABAB graphene implies there will be surface helical edge states at the interfaces of the two systems.

MEAN-FIELD TREATMENT OF THE CORRELATION

Here we analyze the effect of correlations on the density of states at the A sites of the topmost layer. We use a tight-binding model with Hamiltonian $H = H_0 + H_U$ with $H_0 = \sum_{\vec{k},a,b,\sigma} \epsilon_{\vec{k},a,b} c^\dagger_{\vec{k},a,\sigma} c_{\vec{k},b,\sigma}$ the non-interacting part and treat the electron-electron interaction described by H_U within a mean-field approximation. The indices a and b take values $1A, 1B, 2A, 2B, 3A, 3B, 4A, 4B$, where the number indicates the layer (topmost layer: 1, bottommost layer: 4) and A and B label the two sites in the unit cell per layer. In the following we thus represent the dispersion as a 8×8 matrix labeling these different degrees of freedom. In agreement with the ab-initio characterization for the regions being ABCA stacked (main text) we consider

$$\epsilon_{\vec{k}} = \begin{pmatrix} -E_f/2 & f(0,\vec{k}) & 0 & 0 & 0 & 0 & 0 & 0 \\ f(0,\vec{k})^* & -E_f/2 & t' & 0 & 0 & 0 & 0 & 0 \\ 0 & t' & -E_f/6 & f(1,\vec{k}) & 0 & 0 & 0 & 0 \\ 0 & 0 & f(1,\vec{k})^* & -E_f/6 & t' & 0 & 0 & 0 \\ 0 & 0 & 0 & t' & E_f/6 & f(2,\vec{k}) & 0 & 0 \\ 0 & 0 & 0 & 0 & f(2,\vec{k}) & E_f/6 & t' & 0 \\ 0 & 0 & 0 & 0 & 0 & t' & E_f/2 & f(3,\vec{k}) \\ 0 & 0 & 0 & 0 & 0 & 0 & f(3,\vec{k})^* & E_f/2 \end{pmatrix} \tag{S1}$$

while for the ABAB regions we choose

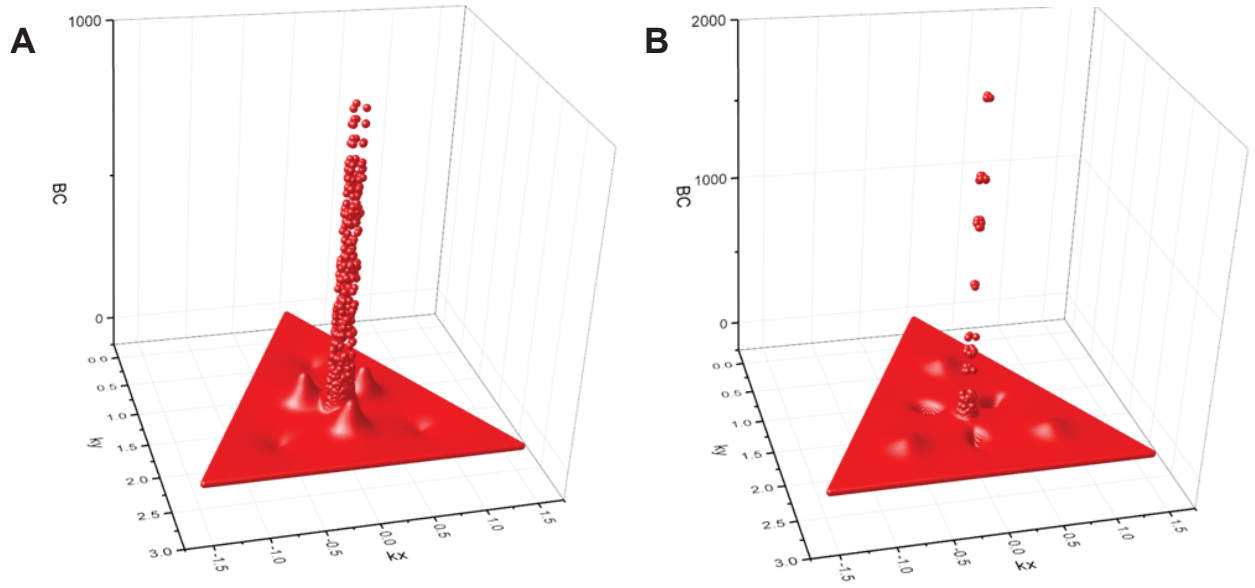

FIG. S2. Berry curvature for the bottom of the ABCA conduction band (A) and ABAB conduction band (B)

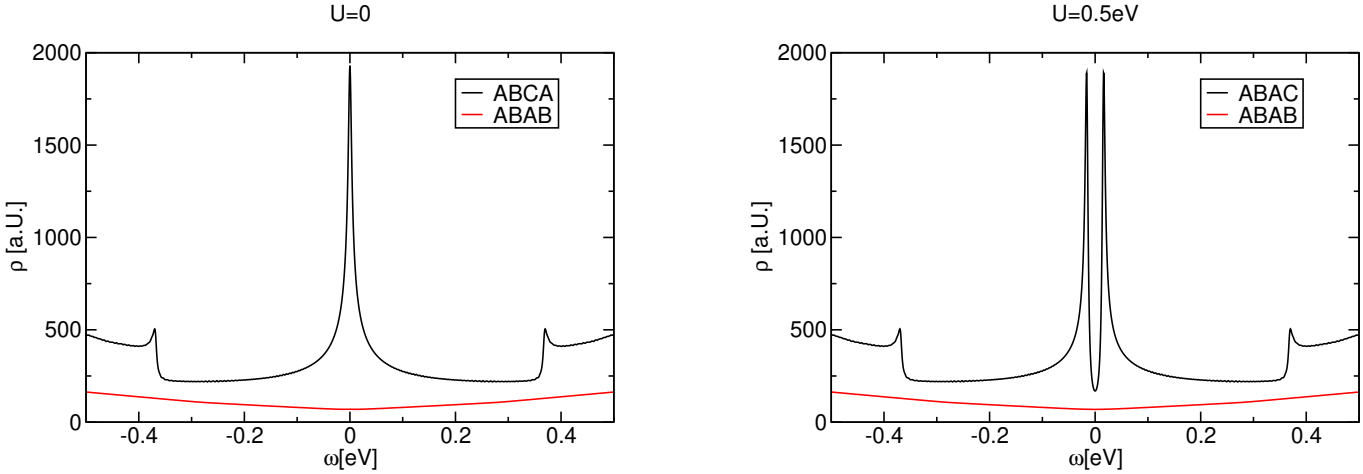

FIG. S3. Left: Comparing the ABAB versus the ABCA non-interacting density of states at the A sites of the topmost layer. For the ABCA we find a square root divergence at low frequencies. Right: The same including local interactions U within a mean field approach.

$$\epsilon_{\vec{k}} = \begin{pmatrix} -E_f/2 & f(0,\vec{k}) & 0 & 0 & 0 & 0 & 0 & 0 \\ f(0,\vec{k})^* & -E_f/2 & t' & 0 & 0 & 0 & 0 & 0 \\ 0 & t' & -E_f/6 & f(1,\vec{k}) & 0 & t' & 0 & 0 \\ 0 & 0 & f(1,\vec{k})^* & -E_f/6 & 0 & 0 & 0 & 0 \\ 0 & 0 & 0 & 0 & E_f/6 & f(2,\vec{k}) & 0 & 0 \\ 0 & 0 & t' & 0 & f(2,\vec{k}) & E_f/6 & t' & 0 \\ 0 & 0 & 0 & 0 & 0 & t' & E_f/2 & f(3,\vec{k}) \\ 0 & 0 & 0 & 0 & 0 & 0 & f(3,\vec{k})^* & E_f/2 \end{pmatrix} \tag{S2}$$

with $f(x,\vec{k}) = t\exp(i\ x\ \vec{k}\cdot\vec{a})[\exp(i\vec{k}\cdot\vec{a}) + \exp(i\vec{k}\cdot\vec{b}) + \exp(i\vec{k}\cdot\vec{c})]$, $t = -3.375eV$, $t' = 0.46eV$, $\vec{a} = (1,0)$, $\vec{b} = (-1/2, \sqrt{3}/2)$, $\vec{c} = (-1/2, -\sqrt{3}/2)$ and where E_f models an electric field applied across the layers. We neglect

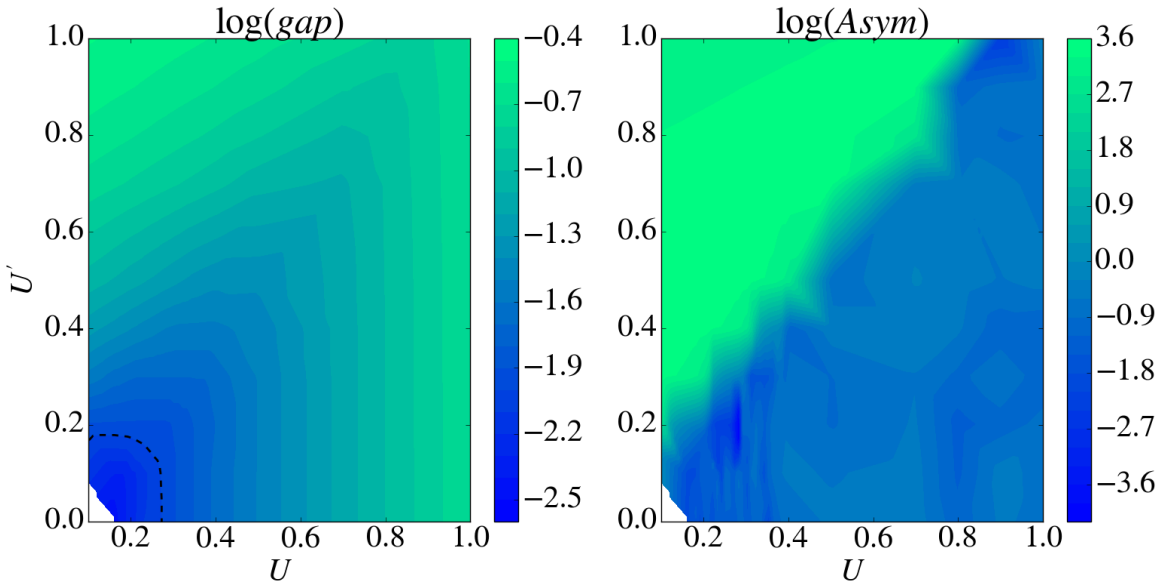

FIG. S4. Characterization of order in the ABCA regions sweeping U and U'. Left: logarithm of the gap size (in meV). The dashed line indicates a gap size of about 10meV. Right: logarithm of the asymmetry of the two peaks in the correlation-split van-Hove singularity. The asymmetry indicates the charge transfer (excitonic) state.

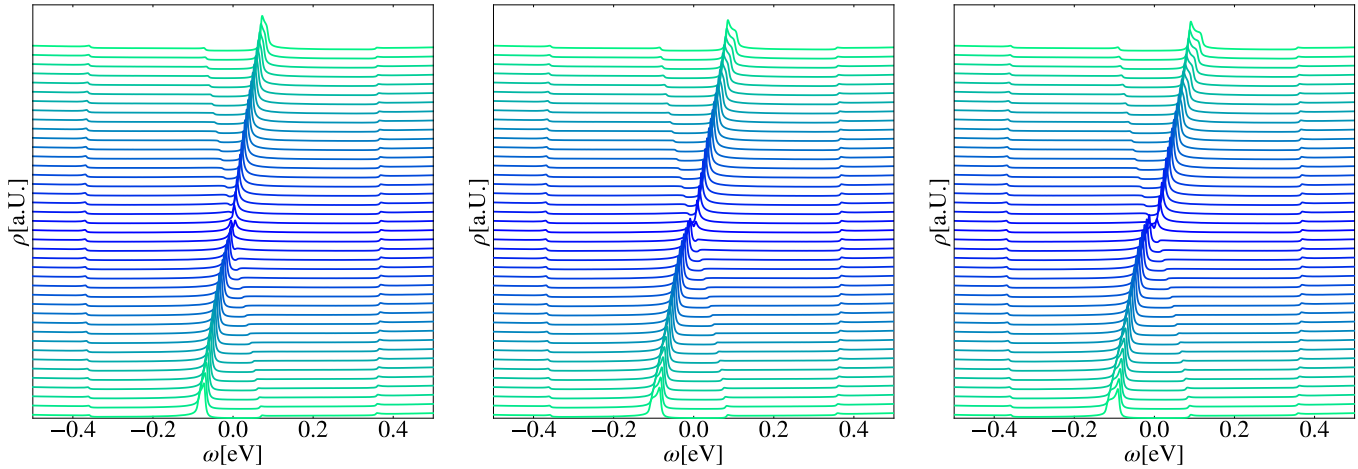

FIG. S5. Waterfall plot of the local density of states including an Electric field sweept from $E_f = -0.2eV$ to $E_f = 0.2eV$ in steps of $0.01eV$ for values which reproduce a van-Hove singularity splitting of about 10meV at $E = 0$. Left: $U = 0.275eV$ and $U' = 0$. Center: $U = 0.2V$ and $U' = 0.175$. Right: $U = 0.1V$ and $U' = 0.2$. $T = 4K$ in all panels.

longer-ranged hoppings across layers for simplicity as they constitute a correction which does not influence the physics we discuss in the following.

The non-interacting density of states at the A sites of the topmost layer is

$$\rho(\omega) \sim \int d^2k \ \ \mathrm{Im}\left[\frac{1}{\omega - \epsilon_{\vec{k}} + i\eta}\right]_{1A,1A} \tag{S3}$$

is shown for $E_f = 0$ in the left panel of Fig. S3 for $\eta = 0.003$.

In the case of ABAB stacking the four low energy bands touch at the Fermi-level in a quadratic fashion (two with positive and two with negative curvature). This gives rise to a constant density of states for $\omega \to 0$ in two dimensions. In contrast the ABCA stacking exhibits a quartic touching point of the two low energy bands (one with positive and one with negative curvature) yielding a divergent density of states $\rho \sim 1/\sqrt{\omega}$ as $\omega \to 0$. This diverging density of states will promote strong correlation effects in the sample. To illustrate this we fist concentrate on a short-ranged

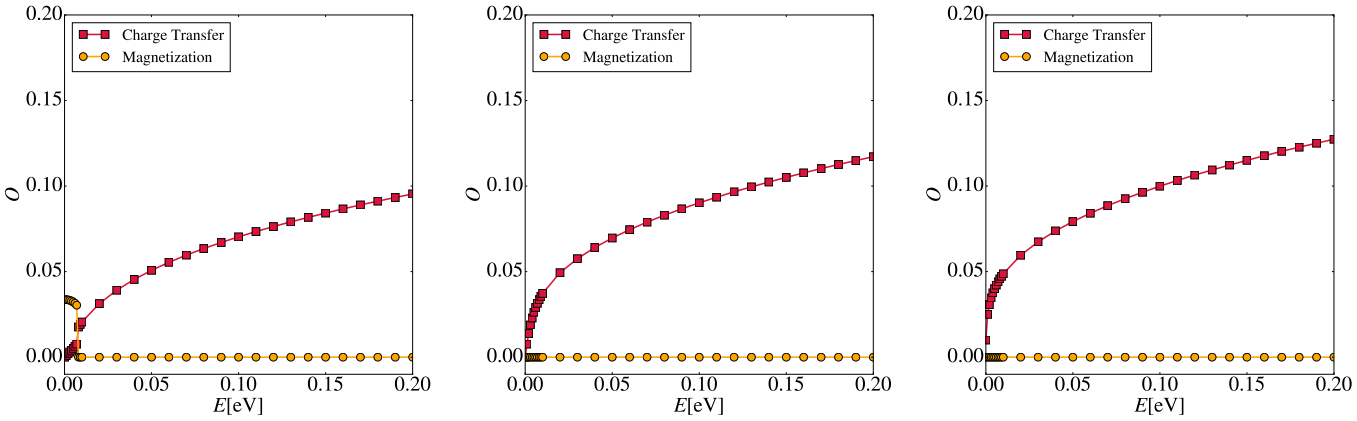

FIG. S6. Order parameter for Ferrimagentic order as well as charge transfer order in dependence of applied electric field for values which reproduce a van-Hove singularity splitting of about 10meV at $E_f = 0$ and $T = 4K$. Left: $U = 0.275eV$ and $U' = 0$. Center: $U = 0.2V$ and $U' = 0.175$. Right: $U = 0.1V$ and $U' = 0.2$.(right)

Hubbard-type interaction between the up and down spin electrons of the material by including

$$H_U = U \sum_i \sum_a \left(n_{i,a,\uparrow} - \frac{1}{2} \right) \left(n_{i,a,\downarrow} - \frac{1}{2} \right) \tag{S4}$$

where i runs over all lattice sites and $n_{i,a,\sigma} = c^\dagger_{i,a,\sigma} c_{i,a,\sigma}$ is the density at site i. The additional terms $-1/2$ are added for convenience and ensure that $\mu = 0$ corresponds to the undoped case. We treat the term H_U in a self-consistent mean-field decoupling and obtain the results shown in the right panel of Fig. S3 for $U = 0.5eV$ and $T = 4K$ (using again $\eta = 0.003$). The effect on the local density of states is minute for the ABAB region, while a prominent splitting of the peaks appears for the ABCA stacking configuration. The correlated (mean-field) state in this case is a Ferrimagnetic state within the topmost layer which spontaneously breaks the $SU(2)$ invariance of the systems and an antiferromagnetic ordering across the topmost and bottommost layer (opposite Ferrimagentic state in the bottommost layer). It is important to note, that the low-energy physics of the ABCA configuration is entirely dominated by the A sites of the topmost and the B sites of the bottomost layers. Since correlations have a negligible effect on the ABAB regions, we will concentrate our discussion of correlations on the ABCA domains in the following.

We do not have an ab-initio or experimental characterization of the precise form and magnitude of Coulomb matrix element. We thus concentrate on the most short-ranged interactions within a layer as well as across topmost to bottommost layer on A and B sites, respectively, as those are the only ones that contribute to the low-energy physics. We therefore concentrate on adding an additional contribution $U' \sum_i \sum_{\sigma,\sigma'} \left(n_{i,1A,\sigma} - \frac{1}{2} \right) \left(n_{i,4B,\sigma'} - \frac{1}{2} \right)$ to H_U to explore the general physics keeping U and U' as parameters to be swept. When turning on U', at values $U' \approx U$, the ferrimagentic state discussed above (at $U' = 0$) gives way to a charge transfer (excitonic) insulating state which spontaneously breaks the inversion symmetry between bottom and top layer, spontaneously transferring charge across the $1A$ and $4B$ sites. In contrast to the Ferrimagnetic state the charge transfer state is compatible with an external magnetic field (which sets an explicit symmetry breaking of the same kind as the spontaneous one of the charge transfer order). A visual representation of these orders in ABCA stacked bi-bi-layer is depicted in Fig. **3e-f** of the main text.

Due to the spontaneous charge transferred, the local density of states at the 1A sites becomes highly asymmetric with respect to ω in contrast to the local density of states in a ferrimagnetically ordered state (see above). We give a full sweep through the U-U' plane keeping $E_f = 0$ in Fig. S4, where we show the gap size (splitting of van-Hove singularities) on the left and the asymmetry (indicating the charge transferred) on the right. Furthermore, we indicate the line of U-U' values where the gap size is about the experimentally reported 10meV.

Next, we analyze the electric field dependence. In Fig. S5 we show the density of states on the A sites of the topmost layer for electric fields from $E_f = -0.2eV$ to $E_f = 0.2eV$ sampled in increments of $0.01eV$. We choose three combinations of $(U, U') = (0.2eV, 0.0)$ (left), $(U, U') = (0.275eV, 0.175eV)$ (center) and $(U, U') = (0.1eV, 0.2eV)$ (right) on the dashed line shown in the left panel of Fig. S4 denoting a splitting of van-Hove singularities of roughly 10meV. Electric field, just as the charge transfer state stabilized by U' tends to separate charges across the bottommost and topmost layer. Therefore at non-zero U' the electric field induced gap in the density of states (and the charge transfer) is stronger.

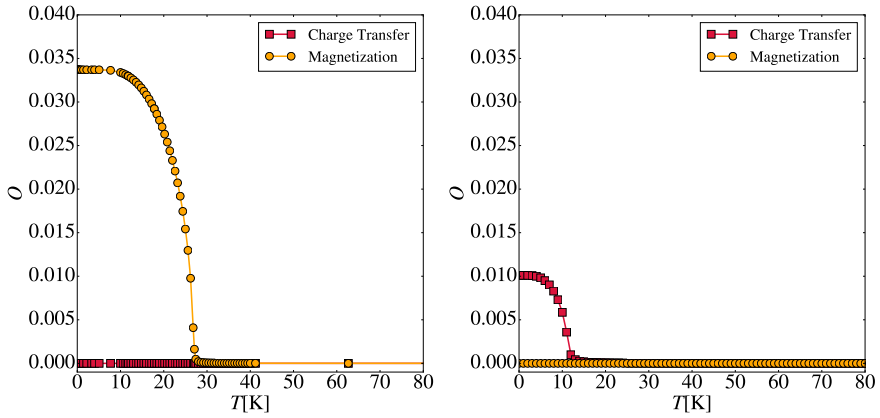

FIG. S7. Temperature dependence of the order parameters for the magnetic and charge order for $U = 0.275$eV and $U' = 0$ (left) as well as $U = 0.1$eV and $U' = 0.2$eV (left) at $E_f = 0$. The mean field critical temperature is approximately $T_C \approx 28K$ and $T_C \approx 12K$ for the two cases.

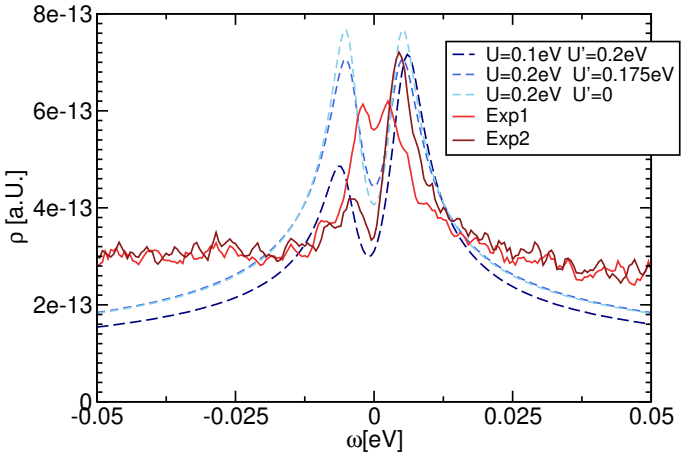

FIG. S8. Comparison of theory to experiment. Experimentally, we concentrate on the most symmetric scenarios for the density of states (labeled Exp2) and the case which is determined to be closest to half-filling and zero applied displacement field (labeled Exp1). The splitting size between the van-Hove singularities is roughly fitted by varying U and U'. The experimental data has a strong tendency to display asymmetric peaks. This indicates that the experimental sample might be (at the verge of) forming spontaneously a charge transfer state even at small E_f.

Next we define the two order parameters for (ferri)magnetic

$$O^{\mathrm{Mag}} = \frac{N_{1A,\uparrow} - N_{1A,\downarrow} - N_{4B,\uparrow} + N_{4B\downarrow}}{N_{1A,\uparrow} + N_{1A,\downarrow} + N_{4B,\uparrow} + N_{4B,\downarrow}} \tag{S5}$$

as well as charge transfer

$$O^{\mathrm{CT}} = \frac{N_{1A,\uparrow} - N_{4B,\uparrow} + N_{1A,\downarrow} - N_{4B,\downarrow}}{N_{1A,\uparrow} + N_{1A,\downarrow} + N_{4B,\uparrow} + N_{4B,\downarrow}} \tag{S6}$$

order, where $N_{a,\sigma} = \sum_i n_{i,a,\sigma}$. Results for these order parameters are shown in Fig. S6 for $(U, U') = (0.2eV, 0.0)$ (left), $(U, U') = (0.275eV, 0.175eV)$ (center) and $(U, U') = (0.1eV, 0.2eV)$ (right). Charge transfer competes with the magnetic order and is stabilized by finite electric field as one would expect. At large $U' > U$ charge transfer can be spontaneous breaking the underlying inversion symmetry (see right panel).

The temperature dependence of the order parameter shows the typical mean-field behavior illustrated in Fig. S7 for $U = 0.275$eV and $U' = 0$ (left panel) as well as for $U = 0.1$eV and $U' = 0.2$eV (right panel) at $E_f = 0$. For $U = 0.275$eV and $U' = 0$ magnetic ordering sets in below a critical temperature of $T_C = 28K$ while there is no charge order for this choice of parameters. On the other hand for $U = 0.1$eV and $U' = 0.2$eV charge ordering emerges at $T_C \approx 12K$ without magnetic ordering.

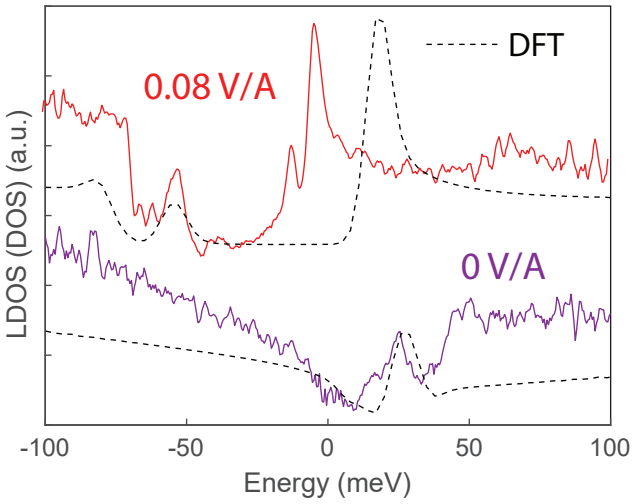

FIG. S9. STS LDOS and DFT top layer DOS at 0 and 0.8 V/nm displacement fields in ABAB graphene.

While experimentally we see that the charge transferred order is more likely due to the asymmetry of the peaks, we do not think that this is definitive evidence for charge transferred order as opposed to Ferrimagnetism – this is left to investigation by future works. Here we take a simple vantage point and compare the most symmetric density of states obtained in the experiment as well as the density of states of the point of near-zero applied displacement field with the $E_f = 0$. Results of the mean field calculation at different combinations of U and U' which roughly reproduce the experimental gap of 10meV are summarized in Fig. S8. Our analysis suggests that the experimental system is likely showing spontaneous charge transfer order.

ABAB FIELD DEPENDENT STS

Figure S9 shows STS LDOS curves on an ABAB domain at 0 V/nm and 0.8 V/nm along with DFT calculated top layer DOS. The experimental and theoretical curves match nicely confirming the ABAB band structure and that a gap opens on the top layer under an applied displacement field.

SWITCHING EDGE STATE ON/OFF WITH GATE ADDITIONAL DATA

Shown in Fig. S10 are STS LDOS maps for several energies at two different gate voltages. At $V_G = +20$ V, both ABCA and ABAB regions are gapped. It can be observed that the edge state only arises within the gap of ABCA graphene, and is absent at other energies which are outside the gap. For comparison, in the bottom panel we show the same STS LDOS energy cuts at $V_G = -20$ V, where a gap is not seen in ABAB graphene in the top layer. No edge states can be seen at this gate voltage for any energy. The data clearly indicates that the emergence of the edge states relies on the presence of a gap on both sides of the interface. The spatial dependence of the edge state also matches exceedingly well with the tight binding calculation for the topological edge state as shown in Fig. 4 of the main text, with the state being localized in the ABCA graphene at a distance of abouts 10 nm away from the actual boundary.

These spectroscopic images also rule out band bending (or other phenomena such as strain-induced bandstructure modification) as a possible explanation for the edge states. If band bending were to occur, this would imply that the local density of states would show contrast at energies both inside and outside the semiconducting gap, since the entire spectrum is shifted when band bending occurs. Our data, on the other hand, shows that the edge states only occur within the gap, exhibiting no contrast outside of the gap at the edge. Band bending or strain induced changes to the overall spectrum therefore cannot be an explanation for the effect

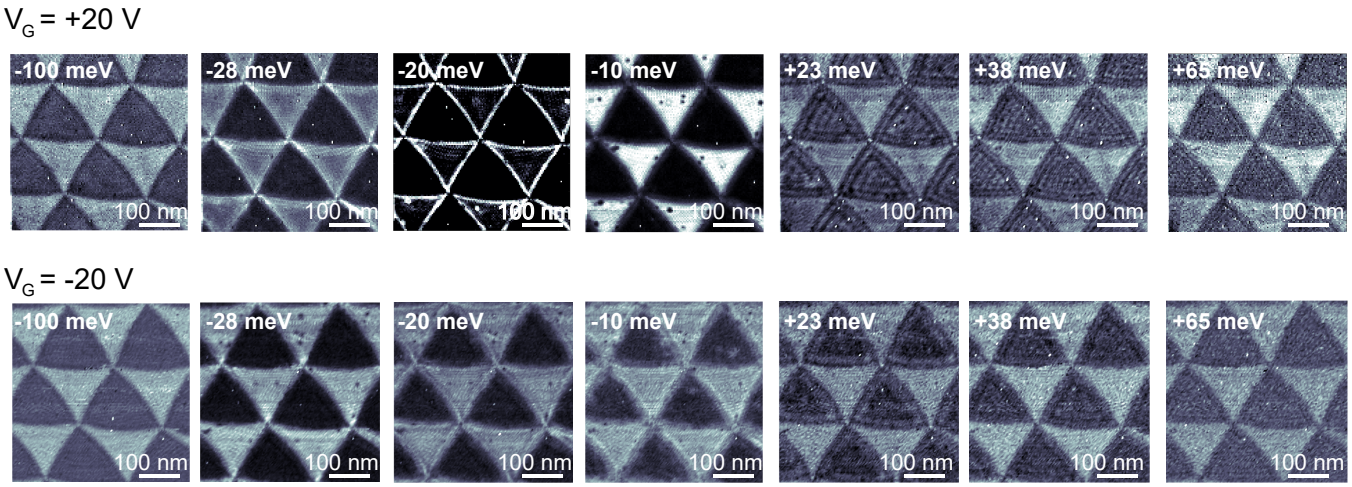

FIG. S10. STS LDOS maps for several energies at V_G = +20 V (top) and V_G = -20 V (bottom).

SUBSTRATE EFFECTS

We further use DFT to study the effect of hBN substrate to the electronic structure of ABCA graphene. With DFT calculations with LDA, we confirm that when a monolayer graphene is placed on top of hBN substrate with perfect alignment, a band gap of 52 meV will be opened in the graphene band structures because of the broken sublattice symmetry. This is consistent with the previous calculations [1]. In the case of ABCA graphene, the sublattice symmetry of each graphene layer is already broken. As shown in Fig, S11(a), the charge density of the flat band states near the Fermi level is located only on one of the sublattices in the top and the bottom layer. The absence of the band gap in the flat band is mainly due to the C2 symmetry of the top and the bottom layers. With the hBN substrate, such symmetry can be broken and a band gap can be opened in the system assuming perfect alignment between the ABCA graphene and the hBN substrate. We calculate the band structures the lowest energy configuration of the ABCA graphene on hBN substrate shown Fig. S11(b). The analysis we present here should be applied to other perfectly-aligned configurations. As shown in the left panel of Fig. S11(d), a small band gap 1 meV is opened in the system without any displacement field, due to the breaking of top and bottom symmetry by the substrate. However, as we increase the negative displacement field, this band gap can be closed (see Fig. S11(d)). The full displacement field dependency of the band gap is shown in Fig. S11(c). Compared with the DFT data shown in Fig. 2(F) in the main text, the position center at which the band gap closes shift from 0.0 eV/nm in the system without substrates to around -0.1 eV/nm with a hBN substrate. With these results, we conclude that since there is no strong coupling between hBN substrate with the ABCA graphene, the effect of the substrate can be understood as a slight shifting of the onsite potential of the bottom layer with respect to the top layer. Therefore, the band gap can always be closed by certain negative displacement field. This conclusion should be generally applied to other perfectly-aligned stacking configurations between the ABCA graphene and the hBN substrate. In the case of misalignment, the effect of the hBN substrate will be even weaker. However, these results in the DFT-LDA calculations are in contrast with the experimental observations. Therefore, a more detailed study involving possible electron-electron correlation as suggested in the main text is required.

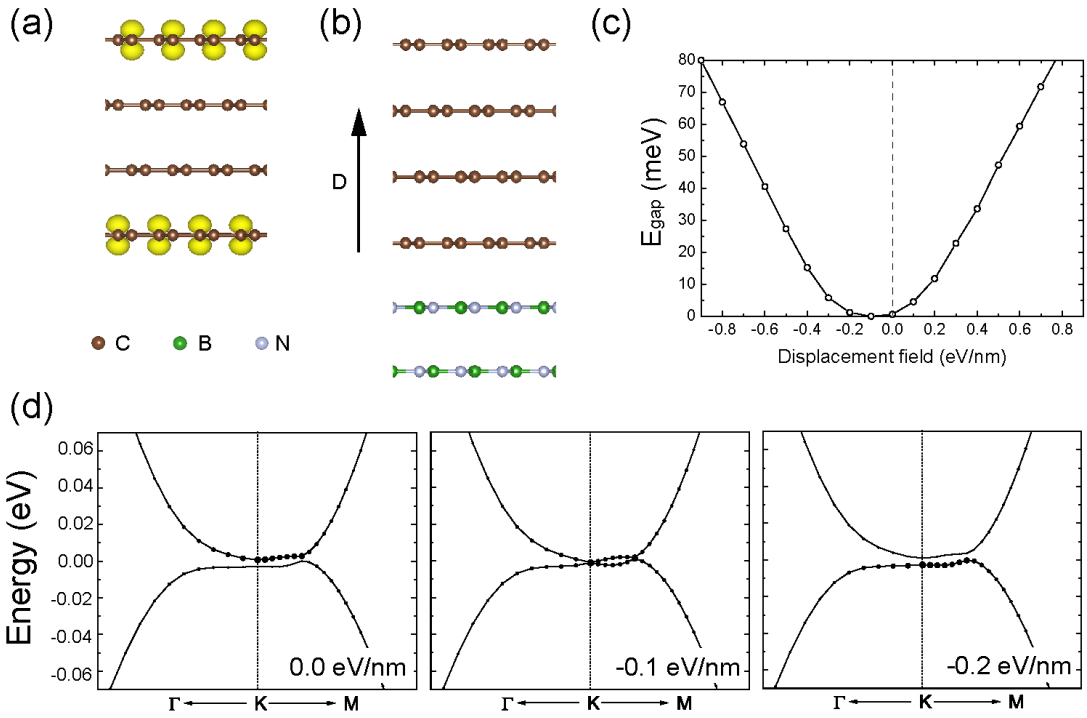

FIG. S11. Band structures of ABCA graphene on hBN substrates. (a) Charge density distribution of the flat band states near the Fermi level in ABCA graphene without substrates. (b) Atomic structures of the lowest energy configuration of ABCA graphene on hBN substrate assuming perfect alignment. The arrow on the left indicates the direction of the external-applied displacement field. (c) Band gap variations of ABCA graphene on hBN substrate under different displacement fields calculated with DFT with LDA pseudopotentials. (d) DFT calculated band structures of ABCA graphene on hBN substrates with increasing negative displacement fields. The size of the black dots is proportional to the projection of the wavefunctions onto the top layer.

[1] Gianluca Giovannetii, 'Substrate-induced band gap in graphene on hexagonal boron nitride: Ab initio density functional calculations', Physical Review B **76**, 073103 (2007)
.